Potential of double pilot injection strategies optimized with the design of experiments procedure to improve diesel engine emissions and performance

(Article begins on next page)

POTENTIAL OF DOUBLE PILOT INJECTION STRATEGIES OPTIMIZED WITH A DESIGN OF EXPERIMENTS PROCEDURE TO IMPROVE DIESEL ENGINE EMISSIONS AND PERFORMANCE.

d'Ambrosio, S. , and Ferrari, A.*

Energy Department – Politecnico di Torino

C.so duca degli Abruzzi, 24, 10129, Torino, Italy.

ABSTRACT

The potential of pilot-pilot-main triple injection strategies versus engine out emissions, combustion noise and brake specific fuel consumption has been assessed experimentally on a Euro 5 diesel engine with a reduced compression ratio (16.3:1). The engine has been fueled with conventional diesel fuel. The experimental tests on the engine have been carried out in a dynamometer cell under different steady state working conditions, that are representative of passenger car engine applications over the European homologation cycle. Furthermore, in-cylinder analyses of the pressure, heat-release rate, temperature and emissions have been performed in order to obtain more detailed knowledge on the cause-and-effect-relationships between the implemented injection strategies and the results of the experimental tests.

The implemented double-pilot injection engine calibrations have been optimized by means of the design of experiments procedure. The plotted data of the engine performance and emissions have been compared with data from the original double-injection schedule, characterized by a retarded main injection timing, in order to intensify the premixed combustion phase. The benefits and the disadvantages of the *PCCI* concept are preliminarily discussed, on the basis of the experimental pilot-main injection strategy results.

The substitution of the pilot-main injection schedule with the triple injection, for light engine loads and low engine speeds, has led to higher combustion pressures, lower heat release rates, shorter ignition delays and lower brake specific fuel consumption. Above all, a significant improvement in engine noise and in both *CO* and *HC* engine-out emissions has been achieved and the NO_x emission have been limited by the application of high *EGR* rates. When medium engine loads and speeds are analyzed, the considered double-pilot injection strategy allows the NO_x emissions to be reduced, compared to the baseline pilot-main injection schedule. However, the combustion noise does not improve and the soot deteriorates, even though the soot penalties are not relevant.

* Corresponding author e-mail address: alessandro.ferrari@polito.it.

Keywords: pilot injections; design of experiments; partial premixed charge compression ignition engines.

Highlights:

- The benefits and the weak points of the partial *PCCI* strategy for low loads and speeds are discussed.
- The effects of the triple pilot-pilot-main injection on engine-out emissions and noise are analyzed.
- The experimental tests on the multiple injections are supported by numerical in-cylinder analyses.

1. INTRODUCTION

The implementation of a pilot injection in diesel engines makes the entire amount of the fuel chemical energy be released over a prolonged time interval, thus determining a longer combustion than for the single injection case. Furthermore, the premixed combustion of some of the pilot injected fuel causes a slight increase in the in-cylinder gas pressure and temperature [1] before the main injection has occurred, and therefore leads to a considerable reduction in the ignition delay of the main injection [2]. This reduction in the fuel ignition delay limits the impact of the premixed combustion and generates a less rapid heat release rate [3] during the main injection than in a single injection schedule [4]. As a consequence, the main combustion becomes predominantly mixing-controlled [3].

A pilot injection that is sufficiently close to the main injection has the potential of enhancing combustion efficiency and thus brake specific fuel consumption (*bsfc*), because the pilot and main combustions are linked smoothly [5]. Pilot injections are also effective in decreasing combustion noise (*CN*), especially at engine idle [3]. Reductions of up to 5-8 dB are generally obtained in the *CN*, compared to single injection strategies [6-8].

Since the pilot injection decreases the impact of the overall premixed combustion, it makes the highest flame temperatures diminish and, as a consequence, the NO_x emissions generally also reduce, compared to the single-injection strategy [9]. However, large pilot injected quantities make the NO_x produced in the pilot combustion grow, and the increase in the NO_x amount produced by the pilot combustion can surpass the decrease in the main combustion NO_x emissions, due to the shortened ignition delay [10]. Furthermore, when heavy *EGR* rates (~60%) are employed, such as in partial *PCCI* strategies, the pilot injection timing and mass do not influence the NO_x emissions to any appreciable extent because the NO_x emissions are very small [5].

The smoke emission in pilot-main injections generally tends to increase, compared to single injections. In fact, the pilot injection increases the in-cylinder temperature and decreases the oxygen concentration in the gases before the main injection has occurred. Both of these effects generally make the smoke emission grow: the increased temperature mainly acts by reducing the lift-off length, which pertains to the main injection, with a subsequent increase in the equivalence ratios close to the nozzle. The insufficient mixing of fuel with air, which is also due to the shortened ignition delay of the main injection, augments the percentage of the diffusion combustion in the main combustion and, as a consequence, the final soot level grows [11]. In general, the quantity of the pilot injection should be below a certain threshold (a general value of 4 mg is normal) in order to contain the smoke number [12].

Finally, *HC* and *CO* emissions reduce at low loads if a pilot injection is implemented~~,~~ because the occurrence of overmixing is ~~more~~ less likely. In particular, the *CO* conversion rate improves because of the relatively high in-cylinder temperature and the shorter ignition delay of the fuel injected in the main injection [4].

The pilot injection can be exploited in different ways to improve engine-out emissions, *CN* and fuel consumption, depending on the working condition [13]. Soot emissions are not relevant at low engine speeds and loads, NO_x and noise are usually controlled, at these conditions, by means of adequate *EGR* rates. The pilot injection is generally optimized, on the basis of the *EGR* rate, in order to reduce *HC* and *CO* emissions [14], which tend to be high, due to the presence of lean and cool regions. The *HC* and *CO* emission situation becomes worse at engine cold start and warm-up, when the oxidation catalyst has less conversion efficiency. Soot, NO_x, noise and *bsfc* are the dominant problems at medium load conditions, that is, in the higher load zone of the *NEDC* region, whereas *HC* and *CO* are not of great concern. Pilot injections are therefore used in these conditions to improve PM-NO_x and $bsfc$-NO_x trade-offs and, above all, *CN* [15].

Pilot injection is generally applied to the *NEDC* area, but it can also be used for other purposes and offers other benefits. An early pilot injection can be applied to increase the in-cylinder pressure at the end of the compression stroke during engine cranking, thus reducing the engine start time. Furthermore, pilot-main injection patterns reduce the cycle-to-cycle variability of the torque, compared to single injections [4], and this induces more stable engine operation, especially after the engine crank phase [16]. Finally, pilot injection can be used at full load to limit the peak in-cylinder pressure and the engine exhaust temperature. The noise due to combustion is less important at these engine working conditions, since other sources of noise dominate in the vehicle, and the pilot injection therefore allows either the fuel rate to be increased or the mechanical and thermal stresses in the engine to be reduced, thus providing possible weight savings or simplifications of the cooling circuit. Instead, when the maximum torque is smoke limited, an early pilot injection can increase the full load torque by improving the utilization of the air within the cylinder, compared to the case of a single injection with a long energizing time [17]. In general, the pilot injection shot can also be used at high loads to reduce soot and improve combustion efficiency, since the main injection duration can be shortened.

The fundamental pilot-main injection scheme constitutes the conceptual basis for the development of more sophisticated and advanced multiple injection strategies that can implement multiple pilot injection shots. Pilot-pilot-main injection schedules have been shown to have a great potential toward noise [18, 19], emission [20, 21] and *bsfc* [20, 22, 19] reductions. However, more trials are required to optimize various engine parameters, such as the *EGR* rate, the swirl actuator position, the boost pressure, the dwell-time, the injection timings, the rail pressure and the energizing times of all of the injection shots, and thus to be able to fully exploit these strategies [23]. In the present work, a design of experiment *(DoE*) procedure has been applied to optimize the double-pilot injection engine calibration. This innovative approach allows the effective benefits of this injection strategy to be assessed, since optimized pilot-pilot-main and pilot-main injection engine calibrations are compared. In general, the aims of the double-pilot injection strategy should be selected on the basis of the engine working conditions and the installed aftertreatment devices. The triple injection in the current investigation is principally aimed at minimizing NO_x and combustion noise. Furthermore, the double- and triple-injection strategies are tested under high *EGR* conditions, whereas most of the research on multiple injections has been conducted under low or moderate *EGR* rates (moderate *EGR* rates correspond to EGR fractions up to 30-40%) [24].

2. EXPERIMENTAL FACILITIES AND ENGINE SETUP.

The experimental tests have been carried out on the dynamic test bed installed at the Politecnico di Torino *IC* laboratories. The test rig is equipped with an '*ELIN AVL APA* 100' cradle-mounted *AC* dynamometer, featuring nominal torque and power of 525 Nm and 220 kW, respectively, as well as a maximum speed of 12000 rpm. The facility is capable of full four-quadrant operation with high speed and torque dynamics, as well as the simulation of zero torque and gear shifting oscillations in the drivetrain.

The test facility is equipped with a '*Pierburg AVL AMA 4000*' raw exhaust-gas analyzer, which is basically made up of three analyzer trains. Two of these trains feature the following modules: one heated flame ionization detector for the *THC* analysis, one heated chemiluminescence detector for the analysis of the NO_x, three nondispersive infrared analyzers for the measuring of low as well as high *CO* and CO_2 concentration levels and one paramagnetic oxygen detector for the O_2 levels. These two trains allow the pollutant emissions to be measured simultaneously, upstream and downstream of the aftertreatment system. The third train is made up of a CO_2 concentration detector for the measuring of the CO_2 concentrations in the inlet manifold, in order to be able to calculate the *EGR* mass fraction, which is defined as $X_{EGR} = \dot{m}_{EGR} / (\dot{m}_{EGR} + \dot{m}_a)$, according to the procedure developed in [25].

As far as the particulate matter (*PM*) measurement is concerned, the dynamic test bed is equipped with the following instruments: *AVL 415S* smokemeter, *AVL 439S* opacimeter and *AVL SPC472* Smart Sampler. Finally, an '*AVL KMA* 4000 Methanol' measuring system continuously meters the engine fuel consumption. This system is based on the *AVL PLU* measuring principle of a servo-controlled positive displacement counter, and it can perform measurements over the 0.28-110 kg/h range with a reading accuracy of 0.1% for diesel fuel.

All of the abovementioned measurement devices are controlled by a *PUMA OPEN 1.3.2* automation system, which also includes *ISAC 400* software for the simulation of the behavior of both the vehicle (road load, road gradient and moments of inertia of the driveline components, which are not physically present on the test bed) and of the driver behavior (use of the clutch, accelerator pedal and gear shifting).

The tested engine, the main features of which are reported in Table 1, is a Euro 5 engine fueled with conventional diesel oil. It has been fully instrumented with piezoresistive pressure transducers and thermocouples for the measurement of the pressure and temperature levels at the following locations: upstream and downstream of the compressor, at the inlet manifold, upstream and downstream of the turbine and downstream of the aftertreatment system. Additional thermocouples have also been installed for the measurement of the temperatures downstream of the intercooler, in the four inlet and exhaust runners, as well as upstream and downstream of the *EGR* cooler. Finally, an *UEGO* air-fuel ratio sensor has been located within the exhaust system. The acquisition of all of these time-averaged quantities are directly managed directly by the *PUMA OPEN 1.3.2* system, through a dedicated firewire front-end module, which can manage up to 48 analog input channels with a maximum data capture rate of 5 kHz per channel.

A high-frequency piezoelectric transducer has been installed on the engine cylinder head to measure the pressure time-history of the gases in one of the cylinders, whereas another high-frequency piezoresistive transducer has been used to detect the pressure levels in the inlet runner of the same cylinder in order to reference the in-cylinder pressure. An *AVL 365C* crank-shaft driven encoder generates the time base for an automatic 14 bit data-acquisition system (based on the *AVL* indimodul 620 system), which is capable of acquiring up to 8 channel data with a maximum frequency of 800 kHz per channel. The acquisition system is managed by *AVL Indicom* software, in order to allow both the online analysis of the indicated cycle and data storage operation for post-processing with a validated three-zone combustion diagnostic tool [26]. In this model, the combustion chamber content is divided into three zones: a fuel zone, an unburned gas zone, (containing fresh-air, residual gas and *EGR*) and a burned gas zone obtained from a global stoichiometric combustion process. Ordinary differential mass and energy conservation equations are applied to the three zones and are solved numerically on the basis of the experimental in-cylinder pressure. The model allows the temperatures of the three zones to be predicted as functions of the crank angle. Furthermore, thermal and prompt NO mechanisms are implemented in the code, according to the Zeldovich and Fenimore submodels, respectively. The soot formation is modeled [27] by means of an expression that uses the mean air-fuel ratio over the combustion interval, whereas the soot oxidation rate is modeled using an empirical formula, based on the temperature of the burned gas zone.

3. THE DESIGN OF THE EXPERIMENT PROCEDURE

The tested engine was calibrated by the *OEM* with a double injection strategy, which represented the state-of-the-art pilot-main injection schedule for the considered engine technology.

The *ppM* injection strategies have been optimized by adopting the statistical design of the experiments (*DoE*) technique. The following parameters were considered as the most relevant input variables for the procedure: rail pressure (p_{Rail}), swirl actuator position (*Sw*), dwell times (*DT*) between consecutive injections (DT_2 between the pilot 2 and pilot 1 shots and DT_1 between the pilot 1 and main shots, where pilot 1 is the closest shot to the main injection and pilot 2 the furthest shot from the main injection), main injection timing (SOI_{Main}), the injection quantities in each shot (q_{Pil1} and q_{Pil2}) and the inducted air per stroke and per cylinder (m_a).

Key-points are engine working points (characterized in terms of *bmep* [bar] and speed *n* [rpm]), considered as representative of the engine application to a passenger car over the new European driving cycle. The following key-points were considered for the tested engine ($n\times bmep$): 1500×2, 1500×5, 2000×2, 2000×5, 2500×8, 2750×12 and idle.

Tables 2 and 3 report (second column) the parameter levels that were considered in the variation lists for the optimization of the *ppM* injection schedule at the 1500×2 and 2000×5 key-points. The center and the extreme values of the range that were considered for each parameter were chosen on the basis of preliminary measurements. An appropriate number of levels was selected in order to obtain accurate results with a reasonable number of tests for each variation list. The quantity of fuel in the main injection is set by the test-bench control system in order to guarantee the *bmep* value, and is therefore not present as a parameter in the variation list. The *EGR* ratio affects the emissions at the diesel engine exhaust to a great extent. However, the *ECU* does not evaluate this parameter directly, but can measure m_a (by means of the air mass flowmeter), which is intimately connected to *EGR*. Therefore, the information related to the induced air, m_a, was considered in the variation lists, instead of the *EGR* ratio.

The preliminary variation list was obtained using the Matlab Model-Based Calibration toolbox, setting a V-optimal type design of experiments, which minimizes the prediction error variance, and a full factorial series, as the candidate set, on the basis of the levels shown in Tables 2 and 3. The preliminary variation list was then randomized and replications of the central point (defined by the center value of each parameter range) were added every 10-15 points in order to further reduce the prediction error variance and check for any possible drifts of the output variables for fixed input parameters. The final variation lists were made up of 120-150 tests for each considered key-point. Once the variation list tests had been carried, it was possible to obtain quadratic models of the output variables as functions of the input variables and of their interactions.

The engine-out specific NO_x, *CO*, *HC* and soot emissions, the *bsfc* and the *CN* were considered as the output variables. Different targets can be introduced for the output variables in order to select the best set of values for the input variables at each key point, that is, the optimized engine calibration. The optimization procedure consists of a number of constraints on the output variables. These constraints depend on the pollutant emission regulations, on the aftertreatment devices that are installed on the engine, on the CO_2 targets and on aspects related to fun to-drive.

The considered Euro 5 engine was equipped with a diesel oxygen catalyst (*DOC*) and a particulate filter, but no aftertreatment device was designed to reduce the NO_x emissions. The optimization strategy for the triple (pilot-pilot-main) injection schedules, based on the *DoE*, was aimed at minimizing NO_x emissions and at reducing the combustion noise with respect to the pilot-main injection calibration, which was originally implemented in the ECU provided by the engine *OEM*. However, rather severe upper limits were also set for *CO*, *HC* and *bsfc*.

Tables 4 and 5 show the reference values of the output variables for the pilot-main injection strategy and the constraints used for the optimization of the triple injection strategy. The optimum values of the input variables, calculated by means if the *DoE* procedure, are reported in the third column of Tables 2 and 3. *EGR* trade-offs were performed in the neighborhood of the calibration baseline points for both the double and the optimized triple injection strategies in order to compare not only the baseline points of the two calibrations, but also two complete curves.

4. LIGHT LOAD CONDITIONS.

4.1 PCCI-like double-injection strategies

Figures 1-3 report the in-cylinder pressure (p_{cyl}), the heat release rate (*HRR*) and the burned gas temperature (T_b) time histories, respectively, for n = 1500 rpm and *bmep*=2 bar. The continuous curves with square- and circle-symbols refer to X_{EGR}≈50% and X_{EGR}≈28%, respectively (these two operating conditions correspond to high and moderate *EGR* rates), and the same pilot-main (*pM*) strategy is adopted in both cases. Since the injection strategy is the same, these preliminary tests are aimed at assessing the effect of the *EGR* rate in *PCCI* engines. The p_{cyl} trace has been measured by means of the piezoresistive pressure transducer installed in the combustion chamber, while the *HRR*, and the T_b time histories have been calculated by means of the three-zone combustion diagnostic tool.

A relatively high dwell time between the pilot and the main injection (DT≈1400 μs) has been implemented (cf. Fig. 2) and a vigorous swirl has been applied to promote the air-to-fuel mixing. The heavy *EGR* rate condition that corresponds to $X_{EGR} \approx 50\%$ has been applied in order to prolong the fuel ignition delay and obtain a partially homogeneous mixture before ignition [28]. Fig.1 shows that the in-cylinder pressure decreases as the *EGR* is increased. In fact, both the flow-rate through the turbine and the upstream pressure are reduced when high *EGR* rates are applied to a short-route *EGR* system (cf. also the schematic of the engine in Table 1). As a consequence, the system may not be able to maintain the desired boost level and a decrease in the boost may therefore be experienced at high *EGR* rates, especially for low loads. The decrease in the in-cylinder pressure with increasing *EGR* in Fig. 1 is due to the reduction in the boost pressure and to the increase in the temperature of the cooled *EGR*, compared to the temperature of the fresh air coming from the engine intercooler. Figs. 2 and 3 show that high fractions of cooled *EGR* and retarded main injection timings allow the maximum *HRR* and the T_b peak value to be contained [29], and the ignition delay of both the pilot and main injected fuel to be lengthened, compared to the moderate *EGR* rate condition (X_{EGR}≈28%). In particular, it can be observed that the pilot combustion in the X_{EGR}≈50% case exhibits a two-stage ignition with the presence of both cool and hot flame reactions, whereas single-stage pilot combustion occurs at X_{EGR}≈28%.

The considered pilot-main (*pM*) injection schedule realizes a highly premixed combustion concept, since the main combustion event starts when the main injection has finished. Most of the fuel injected during the pilot and the main shots burns in premixed combustion conditions. The *HRR* peak, related to the diffusive combustion of the main injected fuel, can be seen in Fig. 2 for X_{EGR}≈28%, but vanishes for X_{EGR}≈50%. The advantage of the implemented strategy is that it induces a simultaneous reduction in soot and NO_x emissions, due to the intensified fuel premixing and to the reduced combustion temperature. Fig. 4 shows that both the soot and NO_x emissions decrease when the *EGR* rate is increased progressively, while the other engine parameters remain constant (the contoured triangle symbol represents the *EGR* rate of the baseline pilot-main injection calibration); this behavior, with respect to X_{EGR}, is not observed when more conventional double-injection patterns are applied. Fig. 5 shows the gas temperature at the diesel oxygen catalytic catalyst inlet (T_{cat}) as a function of the *EGR* rate. The experimental points, evaluated as functions of NO_x in Fig 4 and as functions of *EGR* rate in Fig.5, are the same (maximum NO_x corresponds to minimum X_{EGR} and vice versa).

Higher X_{EGR} levels than 50% are in line with partial *PCCI* applications, which intensify the local mixing of the fuel plume and the charge, with the production of a premixed stratified charge. Furthermore, the selected engine compression ratio was ε=16.3, which falls between the typical values of conventional diesel engines (ε=17÷18) and the characteristic values of partial *PCCI* engines (ε=13÷16, [30]). The reduced compression ratio makes the temperature and pressure, which are closely related to NO_x formation, decrease during the compression phase. This enables the fuel spray to penetrate further with more air entrainment, thus contributing to a decrease in the soot [31], which is also due to the increase in the fuel autoignition delay [32, 33]. Finally, a toroidal combustion-bowl was selected, in line with partial *PCCI* applications, since it assures a rapid fuel mixing when combined with a high swirl number, and a large bowl piston diameter was designed in order to reduce the occurrence of wall impingement. However, unlike typical partial *PCCI* combustion diagrams, the pilot injected fuel does not burn together with the main injected fuel, and a pilot combustion event, which is not connected to the main combustion, can be observed in the *HRR* traces reported in Fig. 2. Furthermore, the ratio of the quantity injected in the main shot to that injected in the pilot shot is significantly higher than that usually adopted in partial *PCCI* engines.

Pilot injection quantities with early injection timings, like the typical ones used in early *PCCI* injection strategies (40-50 *BTDC* degrees), can cause the fuel vapor to spread to the cylinder liner, because the in-cylinder charge pressure and density are low for early injection timings and light loads. This leads to overmixed regions and wall quenching phenomena, both of which are important sources of *HC* and *CO* emissions. In addition, the possible spray impingement on the wall surfaces dramatically increases the amount of unburned hydrocarbons [34], dilutes the lubrication oil and causes the fuel consumption to increase to a great extent, since part of the pilot injected fuel is wasted and unable to ignite. For these reasons, the relatively long dwell time in the pilot-main injection pattern, which is reported in Fig. 2, has been introduced by further delaying the main injection rather than by advancing the pilot injection. Since the pilot injection does not occur very early during the piston compression stroke, and the pilot injected quantity is contained (V_{pil}≈1.7 mm^3), wall impingement occurrence is not a concern. Furthermore, the retarded main combustion contributes to the generation of a reduced soot formation rate because the peak in-cylinder temperature around *TDC* is contained and an enhanced soot oxidation rate can be observed during expansion and blowdown phases, due to the raised burned gas temperatures during the last part of the expansion stroke and at the engine exhaust.

The considered *pM* injection pattern features high levels of *HC* and *CO* emissions, due to low-temperature combustion [35] and fuel overmixing, as well as elevated combustion noise, due to the highly premixed combustion. Furthermore, the *bsfc* become worse, compared to the double injection strategies implemented in conventional diesel engines, due to the retarded main injection timing (SOI_{Main}) and the diminished ε value. These drawbacks are of the same typology as those encountered in classic partial *PCCI* engines featuring late injection strategies.

A minimum temperature level of 200°C is necessary at the catalytic converter inlet (T_{cat}) to obtain a satisfactory efficiency of the diesel oxygen catalyst (*DOC*) for the conversion of the high *HC* and *CO* engine-out emissions at low loads. The T_{cat} values in Fig. 5 can be seen to be higher than this threshold for X_{EGR}>45%.

Since the main injected quantity is much larger than the pilot injected mass, the SOI_{Main}, which is equal to 1° *CA ADTC* in Fig. 2, has not been delayed any further, as occurs in typical late *PCCI* injection strategies, in order to avoid an excessive *bsfc* penalty. In fact, the SOI_{Main} varies within the 3-10° *CA ATDC* range for late *PCCI* injection strategies, whereas it is usually in the 5-7° *CA BTDC* range for diesel engines with conventional combustion systems.

4.2 Triple injection strategies.

Figures 6-8 show comparisons of HC-NO_x, CO-NO_x and $bsfc$-NO_x *EGR* trade-off curves obtained for two different engine calibrations in the 45%<X_{EGR}<55% range and at n = 1500 rpm and $bmep$=2 bar. Fig. 9 instead plots the NO_x-X_{EGR} curves for the two strategies. The triangle symbols in Figs. 6-9 pertain to the previously discussed *pM* injection engine calibration, whereas the circle symbols refer to a pilot-pilot-main (*ppM*) injection engine calibration. The contoured line symbols correspond to the baseline calibration points of the two strategies. The triple injection baseline calibration has been obtained with the *DoE* campaign; not only has a pilot shot been added to the injection train of the baseline point of the *pM* calibration, but the rail pressure, injection timings, energizing times and other engine parameters have also been changed. The *SOI* of the pilot 1 and pilot 2 injections are in the 10÷20 cad *BTDC* range for the *ppM* strategy, and are in line with the literature results concerning the best pilot injection timings in triple injections [4].

It can be observed, from Figs. 6-9, that the *DoE* optimized *ppM* strategy generally allows the *CO* and *HC* emissions to be improved at the same NO_x, with respect to the baseline double injection strategy. Furthermore, a slight enhancement can be detected for the *bsfc*-NO_x trade-off. If reference is made to the calibration baseline points, the NO_x engine-out emissions reduce in the *ppM* case (Fig. 9), in line with [36]. However, the NO_x-X_{EGR} curve is virtually the same for the two strategies and the effectiveness of the *EGR* on the engine-out NO_x emissions therefore does not change for either of the two calibrations.

The *ppM* pattern should lead to a decrease in the local air-to-fuel ratio, with respect to time and space, due to the lower global oxygen concentration ($[O_2]_{int}$ =14.9 versus $[O_2]_{int}$=16.0 of the *pM* calibration). The generation of a suitable fuel vapor stratification close to the nozzle reduces the impact of fuel overmixing and wall quenching, and thus decreases the engine out *HC* and *CO* emissions (cf. Figs. 6 and 7). In other words, the pre-combustion, which is due to the introduction of the pilot 1 injection prior to the main injection, plays a role in attaining a sufficient main combustion ignition and in improving the conversion efficiency of the fuel, and thus in enhancing the complete combustion of the main injection. The improvements obtained for the *bsfc*-, *HC*- and *CO*-NO_x tradeoffs, by means of the pilot-pilot-main injection, are in line with the results found in [19-22] for low loads and speeds. In particular, when *EGR* rates close to 50% are applied, two pilot injections are recommended [15] in order to decrease the *HC* emissions.

The p_{cyl} and the *HRR* curves that refer to the calibration baseline points of both the *pM* and the *ppM* strategies are reported in Figs. 10 and 11, respectively. The *pM* curves have been plotted with solid line and triangle symbols, whereas the *ppM* solid line curves are marked with circle symbols. The two-stage autoignition delay of the pilot 2 injection increases for the *ppM* strategy because the pilot 2 injection takes place earlier in the compression stroke, where the charge pressure and temperature are lower. Furthermore, the maximum p_{cyl} value pertaining to the main injection increases when passing from the *pM* to the *ppM* injection schedule, but the *HHR* pilot peaks and the *HRR* main combustion peak reduce when pilot 1 injection is applied because of the decrease in the premixed combustion portion. This evidence on p_{cyl} and *HRR* proves that the combustion performance has improved, and the p_{cyl} and *HRR* trends with the number of injections can be confirmed from those obtained passing from a single injection to one-pilot injection. As can be seen in Fig. 12, the decrease in the maximum *HRR* and the earlier main combustion induce a slight diminution in temperature T_b of the burned gases for $\theta \geq 370°CA$ in the case of the *ppM* strategy. On the other hand, the earlier SOI_{pil2} of the *ppM* strategy advances the time instant at which the burned gas temperature jumps to high levels and, as a consequence, the residence time in which the burned gases are exposed to higher temperatures than 1900 K increases for the triple injection calibration. The NO_x formation rates are very sensitive to flame temperatures above 1900-2000 K [37], but, on the basis of the Kamimoto-Bae diagram, NO_x emissions are only produced for smaller local equivalence ratios (ϕ) than 1.5 [38]. A larger amount of mixture with relatively high ϕ values should be obtained in the fuel spray for the *ppM* strategy, because of the reduced mixing with air and, consequently, the NO_x emissions can reduce. It is the contribution of the main combustion that makes the final levels of NO_x higher for the *pM* injection schedule (cf. Fig. 13).

When the two pilot shots are applied, the *HRR* curve (Fig. 11) remains uninterruptedly higher than zero from the start of the cool flames pertaining to the first pilot injection till the end of the main injected fuel combustion. Fig. 14 shows the crankshaft angle (*MFB50*) that corresponds to a fuel mass burned fraction equal to x_b=0.5, and the diagrams plotted in Figs. 11 and 14 justify the slight *bsfc* improvement, which in Fig. 8 generally results from the application of the *ppM* strategy. In fact, the combustion heat is released closer to the *TDC* in the *ppM* case than in the *pM* one, in part due to the more advanced SOI_{Main}.

The fuel for the *ppM* strategy burns with a more regular combustion rate, as can be seen in Fig.11 and without high-time derivatives in the burned gas mass fraction time history (cf. also Fig. 14). As a consequence, a remarkable decrease in the combustion noise can be expected, and the CN-NO_x curve in Fig. 15 in fact improves significantly for the triple injection strategy, compared to the *pM* injection schedule (reductions of up to 3.5 dB can occur). This is a consequence of the decrease in the dwell times between the consecutive injection shots, compared to the *pM* case. In fact, the reduction in the premixed combustion portion for the *ppM* strategy makes combustion noise decrease. The advanced SOI_{Main} in the *ppM* injection pattern was purposely implemented in order to reduce the combustion noise. The mass fraction of burned fuel, before the start of the main injection in Fig. 14, is equal to 15% and to 12% for the *pM* and the *ppM* strategies, respectively, while the minimum noise condition generally corresponds to approximately 8% [8].

Figures 16 and 17 show the combustion noise Fourier spectra, evaluated at n=1500 rpm and *bmep*=2 bar, for the *pM* and the *ppM* strategies, respectively. The solid bars in each figure refer to the X_{EGR}≈49÷50% case, whereas the hatched bars refer to X_{EGR}≈52÷53%. A frequency range (500÷2000 *Hz*), in which the spectral combustion noise takes on the highest values, exists in each Fourier spectrum. The presence of a pronounced peak zone, which occurs within a narrow frequency band, is more evident for the *pM* diagram at X_{EGR}≈49÷50%, even though the peak zone tends to disappear as the value of X_{EGR} is increased. The presence of a peak zone in the diagrams in Figs. 16 and 17 indicates that there is an overly dominant frequency range in the signal, which gives tonality to the noise. In other words, the higher the peak intensity and the smaller the extension of the peak zone, the more recognizable the combustion noise as a specific noise. The sensitivity of the combustion noise to *EGR* variations is limited for the *ppM* strategy, while the tonality is more reduced for the *pM* pattern as the *EGR* passes from X_{EGR}≈50% to X_{EGR}≈53%. Since the human ear is very sensitive to changes in noise, a triple injection can contribute to a less irritating perception of the combustion noise when the *EGR* rate is modified.

Finally, the increase in soot emissions, which can be observable in Figs. 18 and 19 for the triple injection, is not of real concern since the smoke emissions continue to show relatively low values (Soot<0.31 g/kWh in Fig. 18 and Soot<0.01 mg in Fig. 19), due to the low peak in-cylinder temperatures and the high relative air-to-fuel ratio (λ) for these engine working conditions. The presence of a soot-NO_x trade-off curve, in the case of the *ppM* injection strategy, shows that the combustion does not feature *PCCI*-like behavior, unlike the *pM* case.

All of the previous explanations and conclusions about the effects that the addition of a second pilot injection has on engine emissions, combustion noise and *bsfc* performance have been based on experimental data at *n*=1500 rpm and *bmep*=2 bar, but they can be extended to the whole area for light loads, from low to medium engine speeds. This can be confirmed from the experimental results plotted in Figs. 20-24, which refer to *n*=2000 rpm and *bmep*=2 bar. In particular, the double-pilot injection strategy offers the best potentiality to reduce *CN*, *HC* and *CO* with limited penalties on soot emissions. The *ppM* strategy can also lead to an improvement in the startability of a cold engine, which is a typical problem for low-compression ratio engines. In fact, the longer ignition delay and poorer vaporization of the fuel can inhibit fuel ignition, but double-pilot injections are able to contrast this tendency.

5. MEDIUM-LOAD CONDITIONS.

Figures 25 and 26 report the *HRR* and x_b time histories, calculated at *bmep*= 5 bar and *n*= 2000 rpm for the calibration baseline points of the *pM* and *ppM* strategies, respectively. The *pM* strategy in Fig. 25 does not feature any cool flames because the in-cylinder pressure and the temperature values at the pilot injection timing are more elevated than in the *bmep*= 2 bar and *n*= 1500 rpm case. Instead, cool flames are present in the *HRR* diagram pertaining to the *ppM* strategy, due to the early injection timing of the pilot 2 shot. The pilot combustion in the *pM* strategy (cf. the solid line with triangle symbols close to θ≈355° *CA* in Fig. 25) is more vigorous than in the *ppM* strategy (cf. the solid line with circle symbols close to θ≈358° *CA* in Fig. 25), due to the presence, in the former case, of a clear single-stage ignition. On the other hand, since the single-stage ignition delay of the main injected fuel is longer in the *ppM* strategy, the premixed combustion peak at θ≈373° *CA* is higher than in the *pM* case. An appreciable mixing-controlled phase is also present at the end of combustion in both the *pM* and the *ppM* strategies.

Figures 27 and 28 show that the *bsfc* and *CN* have almost the same levels at *bmep*= 5 bar and *n*= 2000 rpm for the two strategies. *HC* (Fig. 29) and *CO* (Fig. 30) become worse for *ppM*, mainly due to the longer autoignition delay, but it should be pointed out that these emissions are not a reason for concern at the considered engine working condition.

Figure 31 shows that the NO_x-X_{EGR} dependence is the same for the two strategies. An appreciable improvement in the NO_x emissions can be observed in Fig. 32 (these data have been obtained from the three-zone model) for the baseline calibration point when passing from the *pM* strategy to the *ppM* one. The differences in the NO_x emissions between the two calibration baseline points could be the result of the different ϕ distributions in the combustion zone, because the peak T_b values and the residence times at higher temperatures than 1900 K are similar for the two calibrations (cf. Fig. 33). Furthermore, the higher premixing degree of the pilot injected fuel for the *pM* injection case makes the NO_x emissions increase significantly in the 350° $CA \leq \theta \leq 370°$ *CA* range, compared to the *ppM* strategy.

A slight deterioration in the soot-NO_x *EGR* trade-off can observed in Fig. 34 for the *ppM* calibration, even though the maximum soot values in Figs. 34 are not critical, when a diesel particulate filter is mounted. In general, the increased soot emissions represent a penalty for the considered *ppM* strategy for medium load and speed conditions (the soot values in Fig. 34 are much higher than in Fig. 18). Any diminution in the ignition delay, for conventional diesel combustion, causes an increase in soot emissions, and the addition of the pilot 1 injection contributes to the reduction of the fuel ignition delay [4]. The liquid fuel injected during the pilot 1 shot and during most of the main injection burns in the presence of combustion flames for the *ppM* strategy, and this interference between the liquid jet and the fire is a remarkable source of soot (cf. Fig. 35), which cannot be balanced by the soot oxidation that occurs during the expansion stroke, owing to the high temperatures induced by the retarded combustion (cf. Fig. 36). From this point of view, the oxidation capability of the soot reduces in the *ppM* case, during the first part of the expansion stroke, since T_b is slightly lower than in the *pM* case (Figs. 33), but increases in the exhaust manifold, because T_{exh} is significantly higher in the *ppM* strategy (Fig. 36), due to the significant diffusive combustion shown in Fig. 25.

6. CONCLUSIONS.

Pilot-pilot-main injection strategies have been compared with pilot-main injection strategies in a low-compression ratio Euro 5 diesel engine in order to evaluate the possible benefits in engine-out emissions, combustion noise and fuel consumption.

The considered pilot-main injection represents the state-of-the art double injection strategy for the considered engine technology, whereas the parameters of the triple injection strategies have been optimized by means of a *DoE* procedure. This innovative approach has allowed an effective assessment of the double pilot injection strategy in partial *PCCI*-like engine working conditions to be made, since optimized double- and triple-injection engine calibrations have been compared. *EGR* trade-offs have been performed in the neighborhood of the baseline points that refer to both the original double-injection calibration and the triple-injection calibration optimized with the *DoE*.

The research investigation has been performed on the basis of experimental tests that were conducted on the engine, fueled with conventional diesel fuel, in a dynamometer cell. The tests have been carried out at different steady-state key-points that are representative of engine application in a vehicle over the new European driving cycle for passenger cars. The experimental analysis has been supported by numerical results that were derived from the application of diagnostic combustion models to the in-cylinder pressure time history. The main conclusions of the present work are outlined in a synoptic way as follows.

- The application of *EGR* rates close to 50% and of retarded main injection timings allows the NO_x and the soot emissions to be decreased simultaneously in late *PCCI* double-injection strategies, due to an intensified fuel premixing and to a reduced peak combustion temperature. The main drawbacks of these strategies at low loads are the elevated combustion noise, which is due to the highly premixed combustion, and the high *HC* and *CO* engine-out emissions. The high *HC* levels at the engine exhaust are generated because of the presence of overmixing regions and wall quenching phenomena, whereas the high *CO* engine-out emissions are produced by the relatively low in-cylinder temperature and long fuel ignition delay. Furthermore, the engine *bsfc* deteriorates, compared to the double injection strategies implemented in conventional diesel engines, due to the retarded main injection timing and the reduced engine compression ratio.
- The employment of pilot-pilot-main injection strategies at light loads and low speeds induces an increase in the time-averaged value of p_{cyl}, compared to the *pM* injection schedule, but the *HHR* combustion peaks reduce, due to the fuel ignition delay diminution. The *ppM* pattern, when applied to a late *PCCI* injection strategy, leads to an increase in the local fuel concentration, with respect to time and space. The generation of a suitable fuel vapor stratification, close to the nozzle, reduces the impact of fuel overmixing and wall quenching and thus decreases the *HC* and *CO* engine-out emissions. Significant reductions in the combustion noise, of up to 4dB, can be obtained, compared to the double injection schedule. The changes in the *CN* tonality, as the *EGR* rate varies, are more pronounced for the *pM* strategy than for the *ppM* one and this leads, in the latter case, to a less irritating perception of the combustion noise when the *EGR* rate is modified. Finally, slight improvements in the *bsfc*-NO_x *EGR* trade-off can be observed for the case of the *ppM* injection schedule.
- At medium engine loads and speeds, the late *PCCI* pilot-pilot-main strategy optimized with the *DoE* allows the NO_x engine-out emissions to be decreased significantly, compared to the baseline point of the *pM* injection calibration. However, the NO_x-soot trade-off curve of the *pM* strategy is not improved and soot penalties are therefore incurred for the *ppM* baseline calibration point, even though they are acceptable when a diesel particulate filter is mounted. The *CN*-

NO_x, the *bsfc*- NO_x, the *HC*- NO_x and the *CO*–NO_x *EGR* curves do not change appreciably when the second pilot shot is added to the *pM* injection train.

- On the basis of the results of the present work, a *ppM* injection strategy is recommended for low loads and speeds to improve engine-out emissions and noise in low compression ratio engines characterized by high *EGR* rates. On the other hand, *ppM* strategies do not seem to lead to any significant benefits in the higher part of the *NEDC*, compared to optimized *pM* strategies, for the considered engine typology. Nevertheless, the choice of the most efficient calibration for an engine depends to a great extent on the coupling of the combustion system to the aftertreatment devices that are installed on the engine. Therefore, the *ppM* strategy could be considered for medium load and engine speeds in order to minimize NO_x emissions.

7. NOMENCLATURE.

bmep	brake mean effective pressure
bsfc	brake specific fuel consumption
CA	crank angle degree
CN	combustion noise
DT_1	dwell time between the pilot 1 and main injection shots
DT_1	dwell time between the pilot 2 and pilot 1 injection shots
ECU	electronic control unit
EGR	exhaust gas recirculation
HC	unburned hydrocarbons
HRR	heat release rate
m_a	inducted air per engine cycle and per cylinder
$\dot{m}_a$	fresh air mass flow-rate
$\dot{m}_{EGR}$	exhaust gas mass flow-rate
MFB50	angle at which 50% of the combustion mixture has burned
n	engine speed
NO_x	nitrogen oxides
OEM	original equipment manufacturer
p_{cyl}	in-cylinder pressure
p_{rail}	nominal rail pressure level
PCCI	premixed charge compression ignition

PM particulate matter

q_{Pil1} volume of fuel injected in the pilot 1 injection

q_{Pil2} volume of fuel injected in the pilot 2 injection

SOI_{Main} electrical start of the main injection

SOI_{Pil} electrical start of the pilot injection

Sw swirl actuator position

T_b burned gas temperature

TDC top dead center

X_{EGR} mass fraction of exhaust gas recirculation

ϕ equivalence ratio

λ relative air-to-fuel ratio

θ crankshaft angle in the simulations

8. REFERENCES.

[1] Heywood, J. B., 1988, "Internal combustion engine fundamentals", McGraw Hill, New York.

[2] Maiboom, A., Tauzia, X., and Hetet, J. F., 2008, "Experimental study of various effects of exhaust gas recirculation on combustion and emissions of an automotive direct injection diesel engine", *Energy*, 33, pp. 22-34.

[3] Ehleskog, R., Ochoterena, R. L., and Andersson., S., 2007, "Effects of multiple injections on engine-out emission levels including particulate mass from an HSDI diesel engine", SAE paper. 2007-01-0910.

[4] Suh, K. H., 2014, "Study on the twin-pilot-injection strategies for the reduction in the exhaust emissions in a ow-compression engine", *Proc. IMechE Part D: J. of Automobile Engineering*, vol. 228(3), pp. 335-343.

[5] Lee, J. W., Choi, S. M., Yu, S., Choi, H., and Min, K. D., 2013, "Comparison of the effects of multiple injection strategy on the emissions between moderate and heavy EGR rate conditions: part 1-pilot injections", *Journal of Mechanical Science and Technology*, 27(4), pp. 1135-1141.

[6] Tullis, S., and Greeves, G., 1996, " Improving NO_x versus bsfc with EUI 200 using EGR and pilot injection for heavy duty diesel engines", SAE paper No. 960843.

[7] Bhatt, N. M., Rathod, P. P., Sorathiya, A. S., and Patel, R., 2013, “Effect of the multiple injection on the performance and emission of diesel engine. A review study”, *International Journal of Emerging Technology and Advanced Technology*, vol. 3 (3).

[8] Busch, S., Zha, K. and Miles, P.C., 2014, “Investigations of closely coupled pilot and main injections as a mean to reduce combustion noise”, 8th Thiesel Conference, Valencia 9th-12th September.

[9] Han, Z., Uludogan, A., Hampson, G. J., and Reitz, R. D., 1996, “Mechanism of soot and NO_x emission reduction using multiple-injection in diesel engine”, SAE paper 960633.

[10] Yun, H. H., Sellnau, M., Milovanovic, N., and Zuelch, S., 2008, “Development of premixed low-temperature diesel combustion in a HSDI engine”, SAE paper no. 2008-01-0639.

[11] Helmantel, A., and Golovitchev, 2009, “Injection strategy optimization for a light duty DI diesel engine in medium load conditions with high EGR rates”, SAE paper no. 2009-01-1441.

[12] Nishimura, T., Satoh, K., Takahashi, S., and Yokota, K., 1998, “Effects of fuel injection rate on combustion and emission in a DI diesel engine”, SAE paper 981929.

[13] DieselNet, Engine and emission technology online, since 1997, www.dieselnet.com.

[14] Kastner, O., Atzler, F., Juvenelle, C., Rotondi, R., and Weigand, A., 2009, “Directly actuated piezo injector for advanced injection strategies towards cleaner diesel engines” Towards Clean Diesel Engines, TCDE 2009.

[15] Predelli, O., Gratzke, R., Sommer, A., Marohn, R., Atzler, F., Schule, H., Kastner, O., and Nozeran, N., 2010, “Continuous injection-rate shaping for passenger-car diesel engines – Potential, limits and feasibility”, 31st International Vienna Engine Symposium.

[16] Payri, F., Broatch, A., Salavert, J. M., Martín, J.,

2010, “Investigation of Diesel combustion using multiple injection strategies for idling after cold start of passenger-car engines”, *Experimental Thermal and Fluid Science*, 34, pp. 857–865.

[17] Tow, T. C., Pierpont, D. A., and Reitz, R. D., 1994, “Reducing Particulate and NO_x emissions by using multiple injections in a heavy duty D.I. diesel engine”, SAE paper 940897.

[18] Hotta, Y., Inayoshi, M., Nakakita, K., Fujiwara, K., and Sakata, I., 2005, " Achieving lower exhaust emissions and better performance in an HSDI diesel engine with multiple injection", SAE paper no. 2005-01-0928.

[19] Badami, M., Mallamo, F., Millo, F., and Rossi, E. E., 2003, "Experimental investigation on the effect of multiple injection strategies on emissions, noise and brake specific fuel consumption of an automotive direct injection common-rail diesel engine", *International journal of engine research* 4(4), pp. 299-314.

[20] Okude, K., Mori, K., Shiino, S., Yamada, K., and Matsumoto, Y., 2007, "Effects of multiple injections on diesel emission and combustion characteristics", SAE paper. No. 2007-01-4178.

[21**]** Mobasheri, R. Peng, Z., 2012**, "**Investigation of pilot and multiple injection parameters on mixture formation and combustion characteristics in a heavy duty DI-diesel engine", SAE paper 2012-04-16.

[22] Schoppe, D., Zulch, S., Harfy, M., Geurts, D., Jaorach, R. W., and Baker, N., ,2008, "Delphi Common rail system with direct acting injector", MTZ 10/2008, vol. 69, pp. 32-38.

[23] Ricaud, J.C., and Lavoisier, F., 2004, "Optimizing the multipleinjection settings on an HSDI diesel engine" Conference on Thermo- and fluid-dynamics processes in diesel Engines, Valencia, Spain, 11–13 September 2002

[24] Zheng Z, Yue L, Liu H, Zhu Y, Zhong X, Yao M, 2015, "Effect of two-stage injection on combustion and emissions under high EGR rate on a diesel engine by fueling blends of diesel/gasoline, diesel/n-butanol, diesel/gasoline/n-butanol and pure diesel", *Energy Conversion and Management*, 90, pp. 1-15.

[25] d'Ambrosio, S., Finesso, R., and Spessa, E., 2011, "Calculation of Mass Emissions, Oxygen Mass Fraction And Thermal Capacity Of The Inducted Charge In SI And Diesel Engines From Exhaust And Intake Gas Analysis", *Fuel*, n. 90, issue 1, pp. 152-166.

[26] Finesso, R., and Spessa, E, 2014, "A real time zero-dimensional diagnostic model for the calculation of in-cylinder temperatures, HRR and nitrogen oxides in diesel engines. Energy Conversion and Management 79 498–510. http://dx.doi.org/10.1016/j.enconman.2013.12.045.

[27] Baratta M., Catania A.E., Ferrari A., Finesso R. and Spessa E., 2011, "Premixed-Diffusive Multizone Model for Combustion Diagnostics in Conventional and PCCI Diesel Engines", *ASME Trans. Journal of Engineering for Gas Turbines and Power*, vol. 133 n. 10, Art. No. 102801, pp. 1-13.

[28] Fang C, Yang F, Ouyang M, Gao G, Chen L, 2013, "Combustion mode switching control in a HCCI diesel engine, *Applied Energy* 110 (2013) 190–200", http://dx.doi.org/10.1016/j.apenergy.2013.04.060.

[29] Agarwal D, Singh SK, Agarwal AK, 2011, "Effect of exhaust gas recirculation (EGR) on performance, emissions, deposits and durability of a constant speed compression ignition engine". *Applied Energy* 2011;88(8):2900–7.

[30] Kiplimo, R., Tomita, E., Kawahara, N., and Yokobe, S., 2012, "Effects of spray impingement, injection parameters and *EGR* on the combustion and emission characteristics of a PCCI diesel engine", *Applied Thermal Engineering*, vol. 37, pp. 165-175.

[31] Mendez, S., and Thirouard, B., 2008, "Using multiple injection strategies in diesel combustion: potential to improve emissions, noise and fuel economy trade-off in low CR engine", SAE paper 2008-01-1329.

[32] Broath, A., Ruiz, S., Margot, X., and Gil, A., 2010, "Methodology to estimate the threshold in-cylinder temperature for self-ignition of fuel during cold start of diesel engines", *Energy*, 35, pp. 2251-2560

[33] McMillan, D., La Rocca, A., Shayler, P. J., et al., 2008, "The effect of reducing compression ratio on the work output and heat release characteristics of a DI diesel under cold start conditions", SAE Paper No. 2008-01-1306.

[34] Kiplimo R, Tomita, Kawahara N, Yokobe S, 2012, "Effects of spray impingement, injection parameters, and EGR on the combustion and emission characteristics of a PCCI diesel engine", *Applied Thermal Engineering* 37 (2012) 165-175. doi:10.1016/j.applthermaleng.2011.11.011.

[35] Saxena S, Dedoya ID, 2013, "Fundamental phenomena affecting low temperature combustion and HCCI engines, high load limits and strategies for extending these limits, *Progress in Energy and Combustion Science* 39 (2013) 457-488. http://dx.doi.org/10.1016/j.pecs.2013.05.002.

[36] Suh HK, Investigations of multiple injection strategies for the improvement of combustion and exhaust emissions characteristics in a low compression ratio (CR) engine, 2011, *Applied Energy* 88 (2011) 5013–5019. doi:10.1016/j.apenergy.2011.06.048.

[37] Dec, J., and Canaan, R. E., 1998 "PLIF imaging of NO formation in a DI diesel engine", *SAE Transactions*, 107, No. 3, pp. 176-204.

[38] Akihama, K., Takatori, Y., Inagaki, K., Sakaki, S., and Dean, A. M., 2001, "Mechanism of smokeless rich diesel combustion by reducing temperature", SAE paper no. 2001-01-0655.

9. TABLES AND FIGURES

Engine type	2.0L Euro 5
Displacement	1956 cm^3
Bore × stroke	83.0 mm × 90.4 mm
Compression ratio	16.3
Valves per cylinder	4
Turbocharger	Twin-stage with valve actuators and WG
Fuel injection system	Common Rail 2000 bar piezo
Specific power and torque	71 kW/l – 205 Nm/l
EGR system type	Short-route cooled EGR

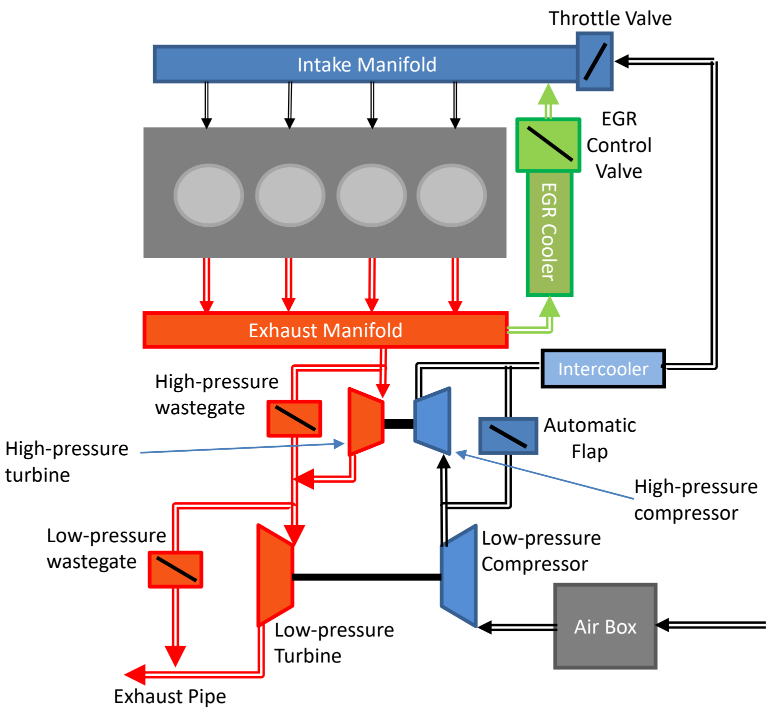

Table 1. Main specifications and schematic of the tested engine.

Quantity	Levels	Optimization
SOI_{Main} [°CA bTDC]	−4.5 −2.88 −1.25 0.37 2	−0.2
m_a [mm^3/(stk·cyl)]	230 245 260	230
Sw [%]	30 38.8 47.5 56.3 65	39.7
p_{Rail}[bar]	300 450 600	516.6
q_{Pil1} [mm^3/(stk·cyl)]	0.8 1.23 1.65 2.08 2.5	1
DT_1 [µs]	300 625 950 1275 1600	446
q_{Pil2} [mm^3/(stk·cyl)]	0.8 1.1 1.4 1.7 2	2
DT_2 [µs]	300 625 950 1275 1600	907

Table 2: Levels considered in the variation list and optimized values of the input variables for the triple injection at 1500×2.

Quantity	Levels	Optimization
SOI_{Main} [°CA bTDC]	−1 1 3	1
m_a [mm^3/(stk·cyl)]	360 380 390 400 420	362.2
Sw [%]	30 38.8 47.5 56.3 65	35.5
p_{Rail} [bar]	750 833.3 950 1016.7 1150	826.4
q_{Pil1} [mm^3/(stk·cyl)]	0.8 1.23 1.65 2.08 2.5	0.8
DT_1 [µs]	300 625 950 1275 1600	773
q_{Pil1} [mm^3/(stk·cyl)]	0.8 1.1 1.4 1.7 2	0.8
DT_2 [µs]	600 850 1100 1350 1600	1600

Table 3: Levels considered in the variation list and optimized values of the input variables for the triple injection at 2000×5.

Strategy	NO_x [g/kWh]	HC [g/kWh]	CO [g/kWh]	Soot [g/kWh]	bsfc [g/kWh]	CN [dBA]
pM	0.53	2	8.8	0.04	299	76.7
ppM	min	≤2	≤9	≤0.3	≤305	≤74

Table 4: Reference values of the reference *pM* calibration baseline point and constraints for the optimization of the *ppM* injection strategy at 1500×2.

Strategy	NO_x [g/kWh]	HC [g/kWh]	CO [g/kWh]	Soot [g/kWh]	bsfc [g/kWh]	CN [dBA]
pM	0.99	0.3	1.9	0.3	248	86.5
ppM	min	≤0.5	≤5	≤1.2	≤255	≤86.5

Table 5. Reference values of the reference *pM* calibration baseline point and constraints for the optimization of the *ppM* injection strategy at 2000×5.

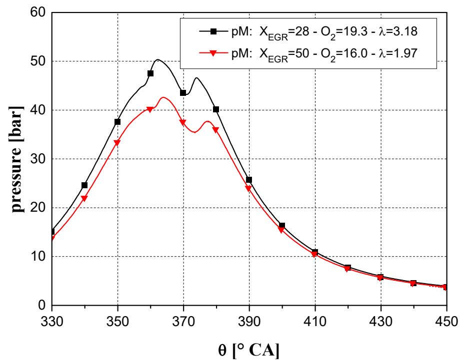

Figure 1. p_{cyl} **versus** θ **distribution for** X_{EGR}**=28% and** X_{EGR}**=50% (*bmep*=2 bar, *n*=1500 rpm).**

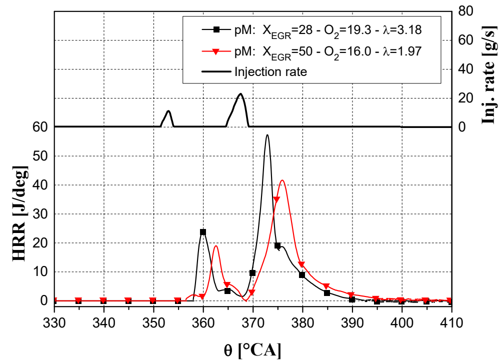

Figure 2. *HRR* **versus** θ **distribution for** X_{EGR}**=28% and** X_{EGR}**=50% (*bmep*=2 bar, *n*=1500 rpm).**

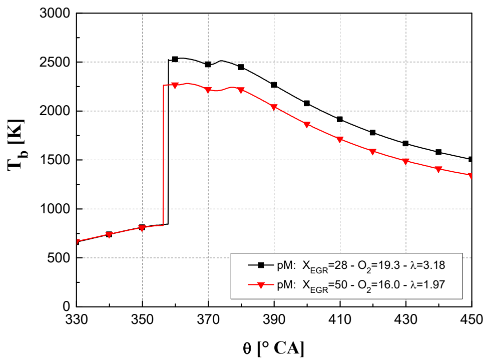

Figure 3. T_b **versus** θ **distribution for** X_{EGR}**=28% and** X_{EGR}**=50% (*bmep*=2 bar, *n*=1500 rpm).**

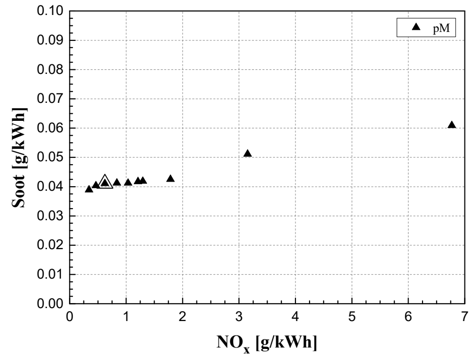

Figure 4.Soot- NO_x **for different** X_{EGR} **values (*bmep*=2 bar, *n*=1500 rpm).**

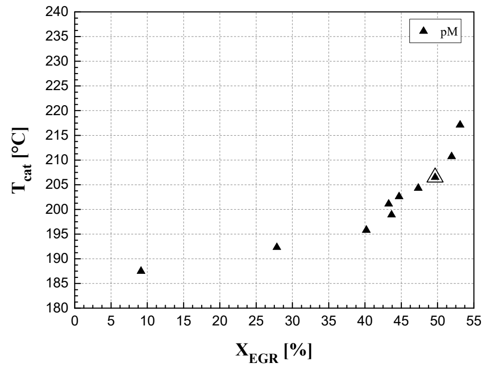

Figure 5. Gas temperature T_{cat} **as a function of** X_{EGR} **(*bmep*=2 bar, *n*=1500 rpm).**

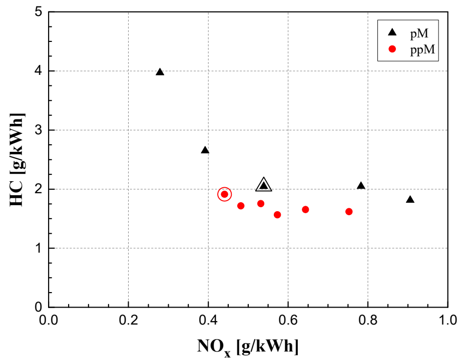

Figure 6. ***HC-NO***$_X$ **trade-off for the *pM* and *ppM* strategies (*bmep*=2 bar, *n*=1500 rpm).**

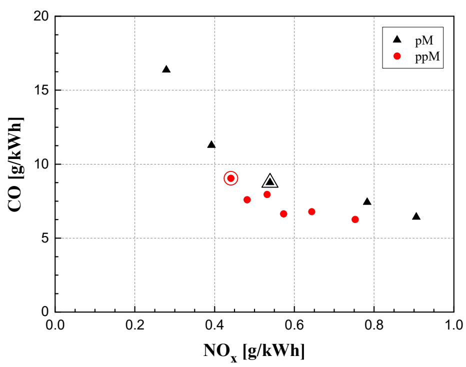

Figure 7. ***CO-NO***$_X$ **trade-off for the *pM* and *ppM* strategies (*bmep*=2 bar, *n*=1500 rpm).**

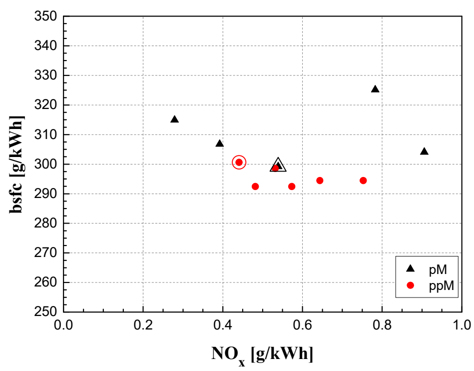

Figure 8. ***bsfc-NO***$_X$ **trade-off for the *pM* and *ppM* strategies (*bmep*=2 bar, *n*=1500 rpm).**

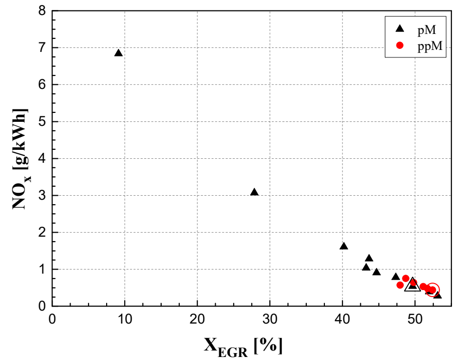

Figure 9. ***NO$_X$*** **versus** ***X$_{EGR}$*** **for the** ***pM*** **and** ***ppM*** **strategies (*bmep*=2 bar, *n*=1500 rpm).**

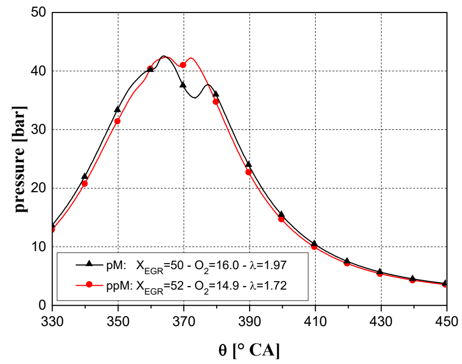

Figure 10. ***p$_{cyl}$*** **versus** ***θ*** **distribution for** ***pM*** **and** ***ppM*** **strategies (*bmep*=2 bar, *n*=1500 rpm).**

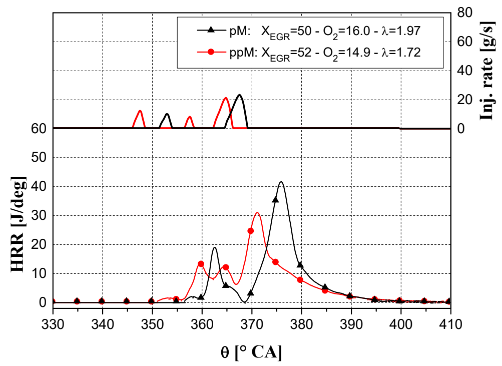

Figure 11. HRR versus *θ* distribution for the pM and ppM strategies (bmep=2 bar, n=1500 rpm)

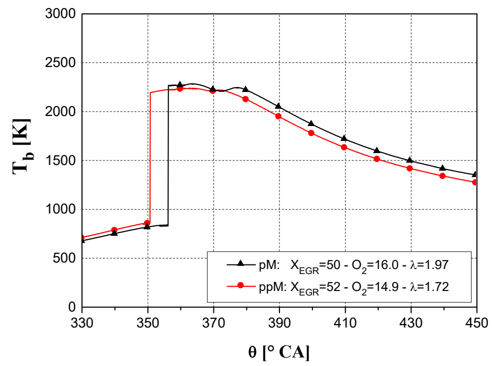

Figure 12. ***T$_b$*** **versus** ***θ*** **distribution for** ***pM*** **and** ***ppM*** **strategies (*bmep*=2 bar, *n*=1500 rpm).**

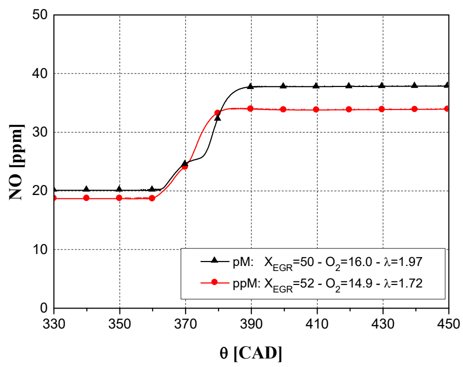

Figure 13. ***NO*** **versus** ***θ*** **distribution for** ***pM*** **and** ***ppM*** **strategies (*bmep*=2 bar, *n*=1500 rpm).**

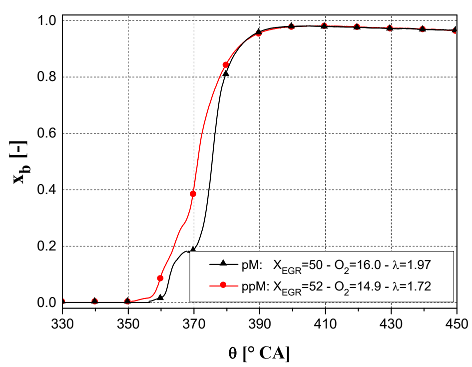

Figure 14. ***x$_b$*** **versus** ***θ*** **distribution for** ***pM*** **and** ***ppM*** **strategies (*bmep*=2 bar, *n*=1500 rpm).**

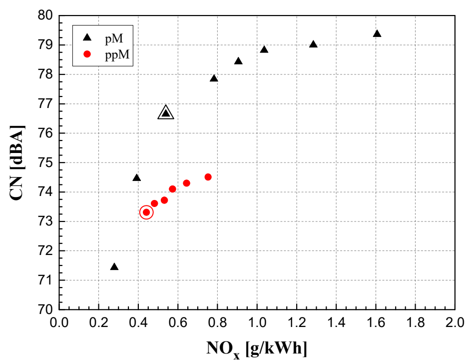

Figure 15. ***CN-NO$_X$*** **trade-off for the** ***pM*** **and** ***ppM*** **strategies (*bmep*=2 bar, *n*=1500 rpm).**

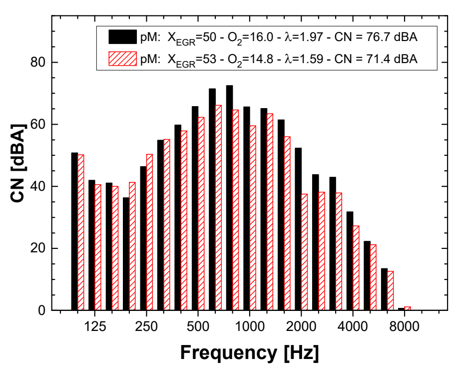

Figure 16. One-third octave frequency bands of *CN* for the *pM* strategy (*bmep*=2 bar, *n*=1500 rpm).

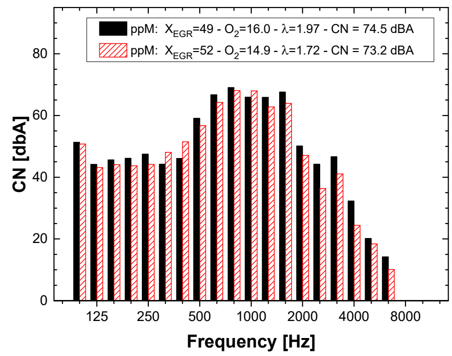

Figure 17. One-third octave frequency bands of *CN* for the *ppM* strategy (*bmep*=2 bar, *n*=1500 rpm).

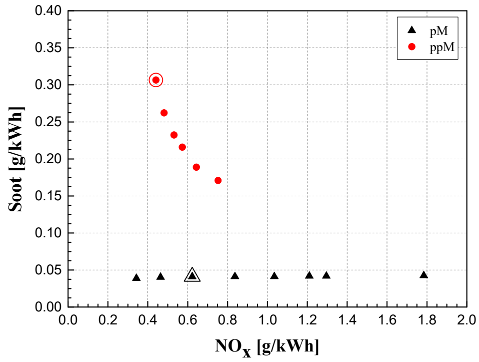

Figure 18. Soot-NO_X trade-off for the *ppM* strategy (*bmep*=2 bar, *n*=1500 rpm).

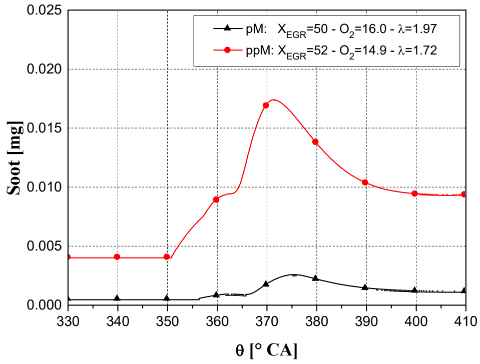

Figure 19. *PM* versus θ distribution for *pM* and *ppM* strategies (*bmep*=2 bar, *n*=1500 rpm).

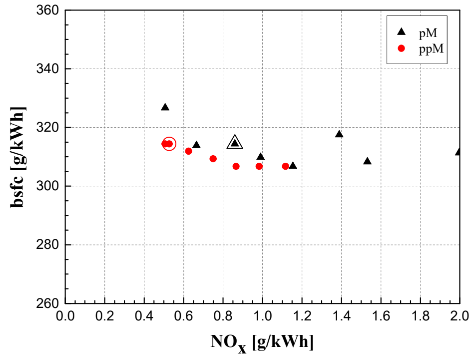

Figure 20. *bsfc*-NO_X trade-off for the *pM* and *ppM* strategies (*bmep*=2 bar, *n*=2000 rpm).

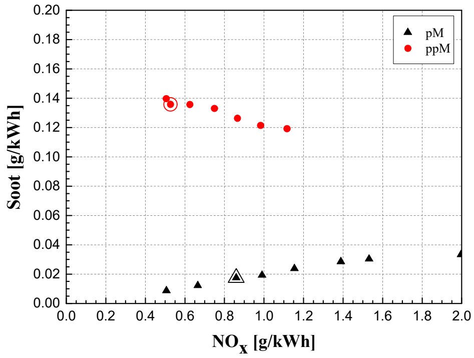

Figure 21. Soot-NO_X trade-off for the *pM* and *ppM* strategies (*bmep*=2 bar, *n*=2000 rpm).

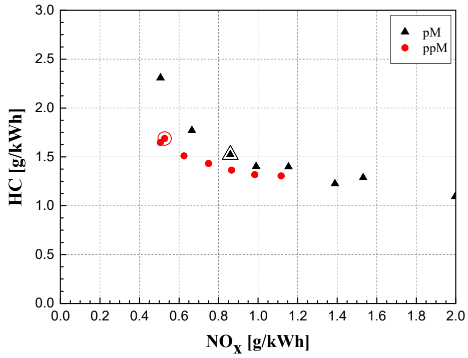

Figure 22. *HC*-NO_X trade-off for the *pM* and *ppM* strategies (*bmep*=2 bar, *n*=2000 rpm).

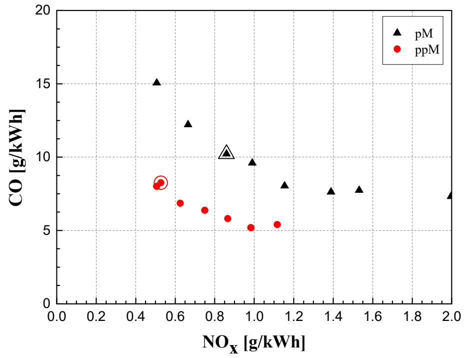

Figure 23. *CO*-NO_X trade-off for the *pM* and *ppM* strategies (*bmep*=2 bar, *n*=2000 rpm).

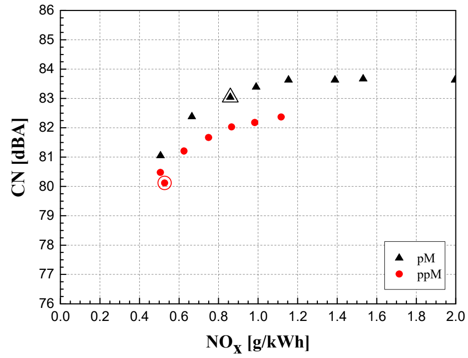

Figure 24. *CN*-NO_X trade-off for the *pM* and *ppM* strategies (*bmep*=2 bar, *n*=2000 rpm).

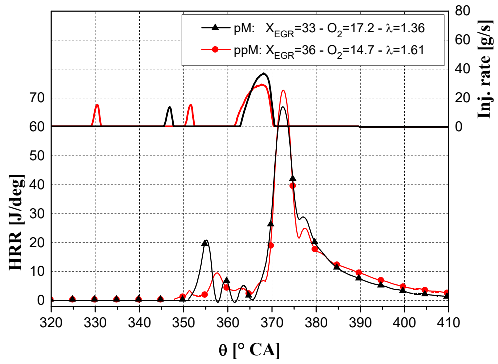

Figure 25. *HRR* versus θ distribution for the *pM* and *ppM* strategies (*bmep*=5 bar, *n*=2000 rpm).

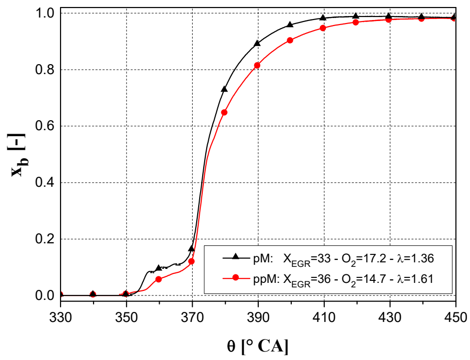

Figure 26. x_b versus θ distribution for *pM* and *ppM* strategies (*bmep*=5 bar, *n*=2000 rpm).

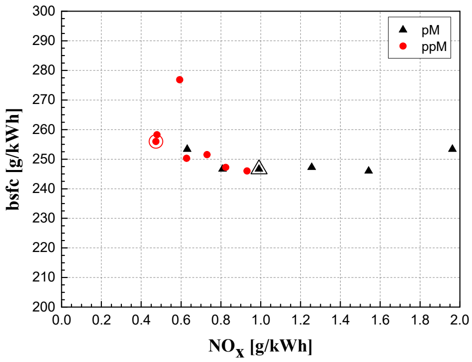

Figure 27. *bsfc-NO$_X$* trade-off for the *pM* and *ppM* strategies (*bmep*=5 bar, *n*=2000 rpm).

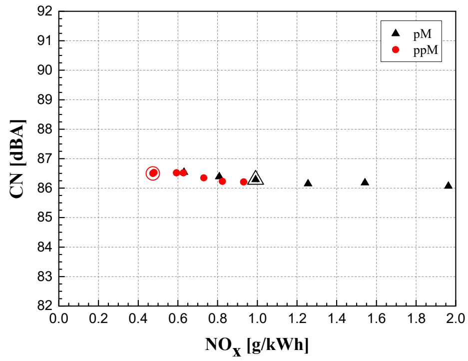

Figure 28. *CN-NO$_X$* trade-off for the *pM* and *ppM* strategies (*bmep*=5 bar, *n*=2000 rpm).

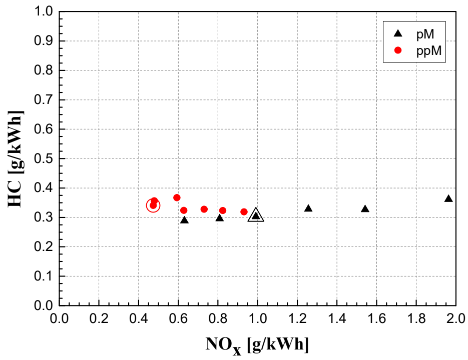

Figure 29. *HC-NO$_X$* trade-off for the *pM* and *ppM* strategies (*bmep*=5 bar, *n*=2000 rpm).

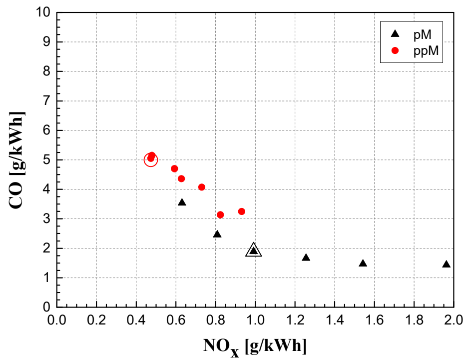

Figure 30. *CO-NO$_X$* trade-off for the *pM* and *ppM* strategies (*bmep*=5 bar, *n*=2000 rpm).

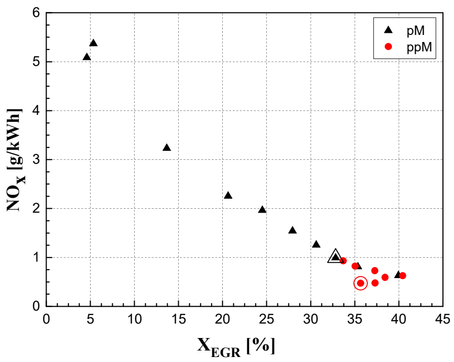

Figure 31. *NO$_x$* versus *X_{EGR}* for the *pM* and *ppM* strategies (*bmep*=5 bar, *n*=2000 rpm).

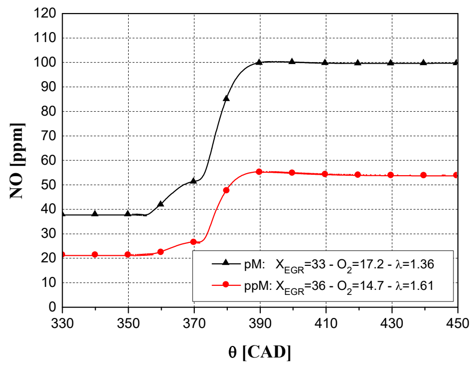

Figure 32. *NO$_x$* versus θ distribution for the *pM* and *ppM* strategies (*bmep*=5 bar, *n*=2000 rpm).

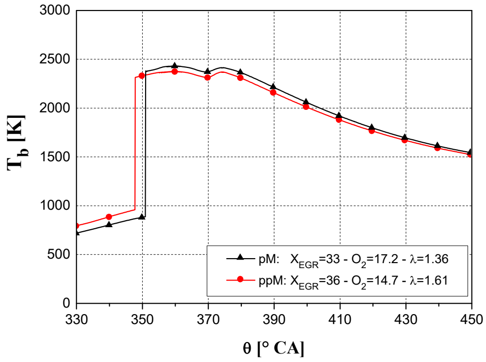

Figure 33. ***T_b*** **versus** ***θ*** **distribution for** ***pM*** **and** ***ppM*** **strategies (*bmep*=5 bar, *n*=2000 rpm).**

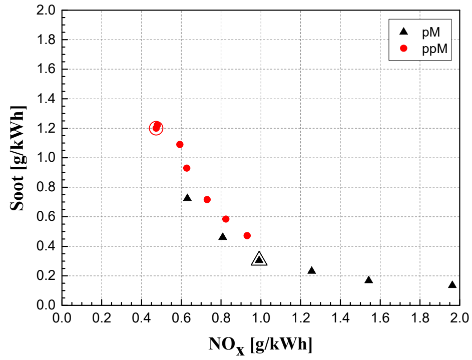

Figure 34. Soot-*NO_X* trade-off for the *pM* and *ppM* strategies (*bmep*=5 bar, *n*=2000 rpm).

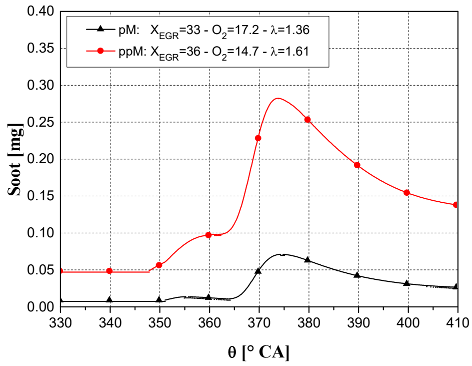

Figure 35. Soot versus *θ* distribution for the *pM* and *ppM* strategies (*bmep*=5 bar, *n*=2000 rpm).

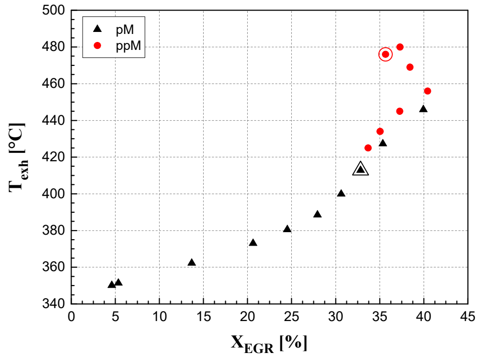

Figure 36. ***T_{exh}*** **versus** ***X_{EGR}*** **for the** ***pM*** **and** ***ppM*** **strategies (*bmep*=5 bar, *n*=2000 rpm).**